PAN
POLISH ACADEMY OF SCIENCES

Opto-Electronics Review

journal homepage: https://journals.pan.pl/opelre

A proposed preamble channel estimation scheme for flip FBMC-based indoor VLC systems

Mohamed Y. El-Ganiny [a*], Ashraf A. M. Khalaf [b], Aziza I. Hussein [c], Hesham F. A. Hamed [d]

[a] Department of Electrical Engineering, Higher Technological Institute, 10th of Ramadan City, Sharqia, Egypt
[b] Department of Electrical Engineering, Faculty of Engineering, Minia University, Minia, Egypt
[c] Electrical and Computer Engineering Department, Effat University, Jeddah, Kingdom of Saudi Arabia
[d] Department of Telecommunications Engineering, Egyptian Russian University, Badr City, Egypt

Article info

Article history:
Received 17 Jan. 2022
Received in revised form 28 Feb. 2022
Accepted 5 Mar. 2022
Available on-line 27 Mar. 2022

Keywords:
Channel estimation; filter bank multicarrier; IEEE 802.15.7 standard; interference approximation method; visible light communication.

Abstract

Filter bank multicarrier waveform is investigated as a potential waveform for visible light communication broadcasting systems. Imaginary inter-carrier and/or inter-symbol interference are causing substantial performance degradation in the filter bank multicarrier system. Direct current-biased optical filter bank multicarrier modulation overcomes all the problems of direct current-biased optical-orthogonal frequency division multiplexing modulation approaches in terms of speed and bandwidth. However, it also wastes a lot of energy while transforming a true bipolar signal into a positive unipolar signal by adding direct current-bias. In this paper, a flip-filter bank multicarrier-based visible light communication system was introduced to overcome this problem. In this system, a bipolar signal is converted to a unipolar signal by isolating the positive and negative parts, turning them to positive and then delivering the signal. Also, a new channel estimation scheme for a flip-filter bank multicarrier system is proposed which improves the channel estimation performance compared to that of each of the conventional schemes. The proposed system performance is measured in terms of bit error rate, normalized mean squared error, and constellation diagram. The superiority of the proposed scheme over other conventional structures has been successfully verified by MATLAB 2020b simulation experiments results. These results are evaluated under indoor visible light communication standard.

1. Introduction

The massive demand for end-user access to various multimedia applications such as high-definition television, live video streaming, audio streaming, video conferences, high-speed internet access, and many other services is fuelling the spectacular rise in mobile data traffic. The demand for a high bandwidth is expected to expand rapidly in the near future in order to provide the aforementioned services [1, 2].

Specifically, as the worldwide demand for this bandwidth grows, the present radio frequency (RF) spectrum will find it increasingly challenging to support many services. Due to the massive increase in latency and decrease in network capacity, this massive increase in data demand has a negative impact on service reliability [2, 3]. Consequently, novel communication-based technologies must be investigated in order to address the RF spectrum congestion problem.

Optical wireless communication (OWC) is one of the solutions that has arisen. OWC led to the birth of a revolutionary communication-based technology known as visible light communication (VLC) [1, 2]. Data transfer via light is not a new concept to humanity. VLC-based systems have recently gained a lot of attention because of the widespread use of light-emitting diodes (LEDs) in various applications. Lower power consumption, longer lighting hours, and the evolution of future lighting systems as LED-based are some of the most notable aspects of LEDs [2, 4]. The most amazing aspect of LED is that it allows for a

*Corresponding author at: mohamed.youssef@hti.edu.eg

https://doi.org/10.24425/opelre.2022.140859
1896-3757/ Association of Polish Electrical Engineers (SEP) and Polish Academic of Sciences (PAS). Published by PAS

simultaneous illumination and communication which has infinite ramifications. This one-of-a-kind feature of LEDs can be used to promote a completely green technology [5–7].

VLC can be considered as attractive and alternative to RF wireless communications because of its large, wide, unlicensed, and unregulated bandwidth in the range of 400 THz to 700 THz. When compared to RF-based wireless communications, this technique offers 1000 times larger bandwidth [5]. The baseband modulation techniques are simple to be implemented in VLC, their use in high-data-rate communication contexts necessitates the use of complicated equalization algorithms. VLC is needed to borrow a robust multi-dimensional modulation scheme such as orthogonal frequency division multiplexing (OFDM) to assure high data transfer rate while also reducing implementation complexity [5–8].

Also, filter bank multicarrier (FBMC) appears to be one of the promising and alternative waveforms for the next generation of mobile networks as it meets the needs of high bandwidth efficiency, low spectral growth, and self-channel equalization [8–13].

Despite all these advantages of FBMC, they come at the expense of the orthogonality which is only applied in the real field. In terms of the so-called intrinsic interference (II), FBMC faces various difficulties [9, 10]. The overlapping between two adjacent sub-channel filters responses will cause II in FBMC which affects the system performance, in particular the BER [9, 11].

On the time-frequency lattice, the purpose of using an offset quadrature amplitude modulation (OQAM) is to eliminate the influence of II by staggering the in-phase and quadrature components. OQAM is unable to prevent intrinsic interference due to the multipath channel complex valued response. Consequently, some hurdles in channel estimation (CE) are required. For preamble and scattered pilot-based training schemes, several FBMC channel estimation approaches have been recently investigated [9, 10].

Preamble-based channel estimation techniques include the interference approximation method (IAM) and the interference cancellation method (ICM) [10, 12]. All IAM pilot structures (IAM-R, IAM-C, E-IAM-C, NPS, and M-IAM) are aimed using interference in a positive way to improve the estimation performance [9–12].

The novelty of this work lies in two main points. First, investigating the effect of applying the conventional IAM preamble schemes in an F-FBMC under VLC channel model (i.e., studied previously for RF systems). Second, a proposed IAM preamble scheme is introduced and compared with the conventional IAM schemes. The performance is evaluated in terms of a normalized mean squared error (NMSE), bit error rate (BER), and constellation diagram.

This paper is organized as follows: section 2 describes the FBMC system model and its mathematical equations; sections 3 and 4 explain the IAM preamble approach and the traditional IAM schemes, respectively. Indoor VLC channel model is investigated via section 5. The proposed system with the novel IAM-preamble scheme is presented in section 6. The results of the simulation and the comparison between the conventional IAM-preamble structures and the proposed one used in F-FBMC under indoor VLC channel model are discussed in section 7. Finally, the conclusion is drawn in section 8.

2. FBMC system model

The conventional FBMC-OQAM system is described in this section, which allows the maximum spectrum utilization due to the overlapping property between neighbouring subcarriers [13, 14]. As shown in Fig. 1, the FBMC system model has OQAM pre-processing, inverse discrete Fourier transform (IDFT), and synthesis filter bank (SFB) on the transmission side, and it also has OQAM post-processing, DFT, and analysis filter bank (AFB) on the reception side. The discrete-time signal at the FBMC synthesis filter bank (SFB) output is given by

$$s(l) = \sum_{m=0}^{M-1} \sum_{n} d_{m,n}\ g(l - n\frac{N}{2}) e^{j\frac{2\pi m\left(l-\frac{l_g-1}{2}\right)}{N}} e^{j\phi_{m,n}}, \quad (1)$$

$$g_{m,n}(l) = g\left(l - n\frac{N}{2}\right) e^{j\frac{2\pi m\left(l-\frac{l_g-1}{2}\right)}{N}} e^{j\phi_{m,n}}, \quad (2)$$

where $d_{m,n}$ represents the real symbols of OQAM, m represents the subcarrier index and n represents the time index of OQAM symbol, $g(l - n\frac{N}{2})$ represents the impulse response of a real symmetric prototype filter, N represents the even number of subcarriers, l_g is a filter length ($l_g = KN$), and K is the overlapping factor.

The subcarrier functions $g_{m,n}(l)$ are only orthogonal in the real field due to the architecture of the pulse (g). Despite excellent frequency and time localization, as well as no channel distortion or noise, there will be some inter-symbol interference (ISI) and/or inter-carrier interference (ICI) at the output of AFB, and this interference is purely imaginary [13].

The imaginary intrinsic interference width is given by

$$\sum g_{m,n}\ (l)\ g^*_{p,q}\ (l) = j\ < g >^{p,q}_{m,n}, \quad (3)$$

where $< g >^{p,q}_{m,n}$ is the interference width between (p, q) and (m, n) frequency and time (FT) points.

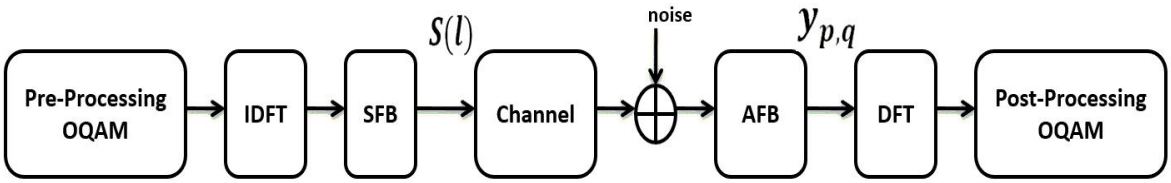

Fig. 1. FBMC/OQAM system model.

Assume that for each subcarrier, all spectral components are passed through the channel with the same gain and linear phase, and that the channel is time-invariant throughout the duration of the prototype filter.

Consequently, the output of AFB at the subcarrier of p_{th} and FBMC symbol of q_{th} is given by

$$y_{p,q} = H_{p,q}d_{p,q} + \underbrace{j\sum_{m=0}^{M-1}\sum_{n}H_{m,n}d_{m,n} < g >_{m,n}^{p,q}}_{(m,n)\neq(p,q)} + \eta_{p,q} \qquad (4)$$

$$I_{p,q}$$

At that FT point, $H_{p,q}$ represents the channel frequency response (CFR), $I_{p,q}$ represents the related interference and $\eta_{p,q}$ represents the Gaussian noise components which have zero mean and variance σ^2.

$$y_{p,q} = H_{p,q}\left[d_{p,q} + j\sum_{m=0}^{M-1}\sum_{n}d_{m,n} < g >_{m,n}^{p,q}\right] + \eta_{p,q} \qquad (5)$$

Due to the good localization in time and frequency of the pulses g, the interference from FT points outside the neighbourhood $\Omega_{p,q}$ of (p,q) is neglected [9, 10, 13].

Consequently, the output of AFB is approximately defined by

$$y_{p,q} \approx H_{p,q}\,C_{p,q} + \eta_{p,q}, \qquad (6)$$

where $C_{p,q}$ is given by

$$C_{p,q} = d_{p,q} + j\cdot u_{p,q}. \qquad (7)$$

$C_{p,q}$ is the virtual transmitted symbol at (p,q), with

$$u_{p,q} = \sum_{(m,n)\in\Omega_{p,q}} d_{m,n} < g >_{m,n}^{p,q}. \qquad (8)$$

The estimated CFR can be defined by

$$\widehat{H}_{p,q} = \frac{y_{p,q}}{C_{p,q}}. \qquad (9)$$

Assume that

$$y_{p,q} = H_{p,q}C_{p,q} + \eta_{p,q}. \qquad (10)$$

By substituting (10) into (9) we get:

$$\widehat{H}_{p,q} = \frac{H_{p,q}C_{p,q} + \eta_{p,q}}{C_{p,q}}, \qquad (11)$$

so, we can update (9) to be

$$\widehat{H}_{p,q} = H_{p,q} + \frac{\eta_{p,q}}{C_{p,q}}. \qquad (12)$$

Transmitting the pilot sequences $C_{p,q}$ at these FT points will approximately estimate the neighbourhood. This can be used as a pseudo pilot to estimate the CFR at the associated FT points.

According to (12), when the magnitude of pseudo pilots $C_{p,q}$ is increased, a better channel estimation is achieved. Also, the noise components $\eta_{p,q}$ will be minimized. The approach of IAM schemes rely heavily on this methodology [9–13].

3. Interference approximation method (IAM)

IAM is one of the preamble-based CE techniques that approximates the intrinsic imaginary interference from adjacent pilots, allowing the construction of complex pilots that can be tuned to the complex CFR [9, 10, 14].

If the interference $u_{p,q}$ in (7) is only attributable to the immediate neighbours of (p,q) and these FT points carry known training symbols, the IAM approach can compute this interference in an approximate manner.

As previously stated, pilot symbols should have the largest possible magnitude. For all frequencies p, the neighbouring pilots must be selected so that all terms in (8) have the same sign. Consequently, they are summed together. [13–15].

For each FT point, $< g >_{m,n}^{p,q}$ is the value of the interference weights between neighbours in position (m,n) and in position (p,q).

These can be calculated a priori using the prototype filter g that is currently in use. For any choice of g, these weights follow a certain pattern, as shown in Fig. 2. The horizontal direction corresponds to time and the vertical direction corresponds to frequency. Figure 2 shows the number of $< g >_{m,n}^{p,q}$ coefficients on the first order neighbours of the point (p,q). The interference weights for the filter are $\gamma = 0.5644$, $\beta = 0.2393$, $\delta = 0.2058$ and $\varepsilon = 0$ with the overlapping factor $K = 4$.

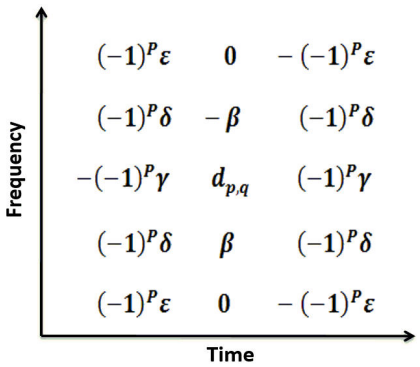

Fig. 2. Interference weights pattern.

In this work, the first-order neighbourhood is considered. $d_{p,q}$ is located in the middle of the preamble. These interference weights should be calculated, the values of those can be computed based on the prototype filter g. γ and β have the highest weights compared to the values of δ and ε.

The above quantities (β, γ, δ and ε) are (absolutely) smaller than one with $\beta, \gamma, \delta > 0$. Generally, $\beta, \gamma > \delta > \varepsilon$.

Table 1 can be used to show the above quantities [10, 13, 15].

Table 1.
Interference weights pattern quantities.

Interference weights pattern quantities	$N = 512$ & $K = 3$	$N = 512$ & $K = 4$
$\beta = e^{-j\frac{2\Pi}{N}\frac{l_g-1}{2}} \sum_{l=0}^{l_g-1} g^2(l)\, e^{j\frac{2\Pi}{N}l}$	0.25	0.2393
$\gamma = \sum_{l=\frac{N}{2}}^{l_g-1} g(l)g(l-\frac{N}{2})$	0.553	0.5644
$\delta = -je^{-j\frac{2\Pi}{N}\frac{l_g-1}{2}} \sum_{l=\frac{N}{2}}^{l_g-1} g(l)g(l-\frac{N}{2})e^{j\frac{2\Pi}{N}l}$	0.2172	0.2058
$\varepsilon = e^{\mp j\frac{2\Pi}{N}(\frac{l_g-1}{2})} \sum_{l=\frac{N}{2}}^{l_g-1} g(l)g(l-\frac{N}{2})e^{\pm j2\frac{2\Pi}{N}l}$	≈ 0.0004	0

4. The traditional IAM schemes

The IAM approach includes many structures such as IAM-R, IAM-C, E-IAM-C, a novel preamble design (NPS) and M-IAM, all of which try to improve channel estimation performance by constructively approximating interference. Figure 3 depicts all these structures, with OQPSK modulation and $N = 8$ [16–20].

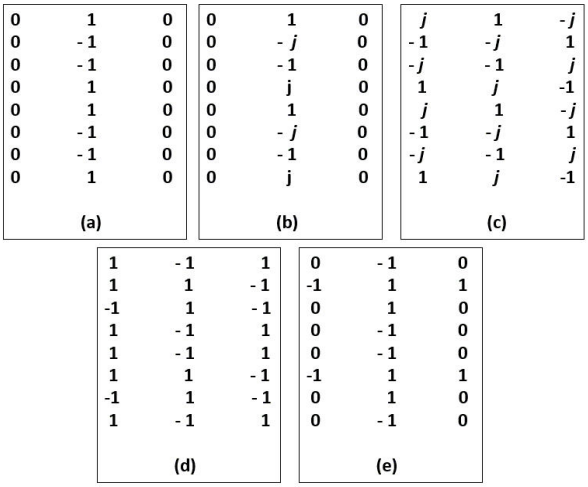

Fig. 3. IAM schemes for: IAM-R (a), IAM-C (b), E-IAM-C (c), NPS (d), and M-IAM (e).

IAM-R is the first IAM scheme which has real training pilots. The first and third columns of this scheme are all nulls as shown in Fig. 3(a) [9, 10, 17].

As shown in Fig. 3(b), pseudo pilots in IAM-C can be real or imaginary at all subcarriers p by setting the column in the middle as in IAM-R, but with the odd indexed subcarriers multiplied by j [9, 10, 18].

E-IAM-C is another structure producing pilots that have a higher magnitude than IAM-C. E-IAM-C structure is shown in Fig. 3(c) [9, 10, 19].

Novel preamble scheme (NPS) is a hybrid of the ICM and IAM schemes. NPS has a larger magnitude than other ICM systems but is smaller than the next schemes [9, 10, 20]. NPS preamble structure is shown in Fig. 3(d).

M-IAM as shown in Fig. 3(e) was proposed based on sending pilots in the positions of γ and β which have the highest weights in comparison to the values of δ and ε. Also, according to the interference weights pattern and to the increase of the pilot magnitude, this structure positions the signs of adjacent pilots [10].

The major and common point for all IAM approaches is to calculate the magnitude of the preamble scheme $C_{p,q}$ to obtain a better channel estimation performance as discussed before.

The magnitude of the preamble pilot equal to the power of $(C_{p,q} = d_{p,q} + ju_{p,q})$ can be defined by

$$\begin{aligned}\text{Magnitude} = \mathbb{E}\Big\{\big|d_{p,1} &+ j\big(d_{p+1,1} < g >^{p,1}_{p+1,1} \\ &+ d_{p-1,1} < g >^{p,1}_{p-1,1} \\ &+ d_{1,q+1} < g >^{p,1}_{1,q+1} \\ &+ d_{1,q-1} < g >^{p,1}_{1,q-1}\big)\big|^2\Big\}. \end{aligned} \quad (13)$$

5. Indoor VLC channel model

An indoor VLC system uses a LED as the source on the transmission side and a large-area photodiode (PD) is used on the reception side. The intensity modulated signal $x(t)$ is passed through the channel environment and received by the PD to attain the signal $y(t)$ [5, 21, 22].

Mathematically, this can be represented as follows:

$$y(t) = R\, x(t) \otimes h(t) + n(t). \quad (14)$$

In (14), R denotes the photodiode responsivity, $x(t)$ and $y(t)$ depict the transmitted and received signal, respectively, $h(t)$ is the channel impulse response, and $n(t)$ denotes the additive white Gaussian noise (AWGN).

Since the instantaneous optical power is proportional to the generated electrical current, VLC channel differs from traditional RF wireless channels.

As a result, the signal $x(t)$ represents power rather than amplitude. Consequently, the transmitted signal has two important constraints. First, the transmitted signal x(t) should have a non-negative value. Second, the maximum amount of transmitted optical power must meet eye safety requirements [5, 22].

The main goal of this section is to figure out the VLC channel impulse response for a single opto-electronic illuminating source scenario.

The signal transmitted by the LED is reflected many times due to the multipath propagation environment, which includes walls, floors, ceilings, furniture, and other objects. Hence, in addition to the line of sight (LOS) component, there are several non-line-of-sight (NLOS) components [22–28].

Here, for simplicity, the NLOS components are ignored and only LOS path is considered. Therefore, the intensity of the received signal is solely determined by the transmitter radiation pattern, photodiode active area, and receiver optics [23, 24].

Other parameters such as dimensions of the room, transmitter and receiver relative position and if the optical intensity of the transmitter is assumed to be P_t, the optical power equivalent to the receiver can be determined as

$$P_R = H(0)P_t\,. \tag{15}$$

The parameter $H(0)$ corresponds to the DC channel gain which is represented as

$$H(0) = \int_{-\infty}^{\infty} h(t)dt\,. \tag{16}$$

If the transmitter is modelled as a generalized Lambertian pattern, then the DC channel gain can be expressed as

$$H(0) = \begin{cases} \frac{A_{PD}\,(m+1)}{2\pi d^2} T_s(\psi) g(\psi) \cos^m(\theta) \cos(\psi), & 0 \le \psi \le \psi_c \\ 0, & \psi \ge \psi_c \end{cases} \tag{17}$$

Lambert's mode number m is a number representing directivity of a light source radiation in space [24, 25]. The relation between m and the LED semi-angle at half-power ($\theta_{\frac{1}{2}}$) can be expressed by

$$m = \frac{-\ln 2}{\ln(\cos\theta_{\frac{1}{2}})}\,. \tag{18}$$

To ensure a successful detection, the received signal must be within the range of the photodiode FOV; otherwise, the received signal will not be detected if it is outside the range of the receiver FOV [21–25]. Consequently, the detector can be modelled as an active area (APD) that collects radiation incident at angles ψ smaller than the FOV of the detector [25–27].

The parameters as presented in (17) and specified in Fig. 4 are shown in Table 2.

In order to derive mathematical expressions for the channel impulse response to LOS, Figure 5 shows the simulation results distribution of the received power related to LOS for an indoor VLC system using a single illuminating source.

Some physical aspects of the room (i.e., location, orientation, and window size) have a major impact.

6. Proposed IAM preamble scheme for F-FBMC-based indoor VLC system

The proposed IAM preamble pilots have all real values which makes them simple compared to IAM-C and E-IAM-C.

As shown in Fig. 6, pseudo pilots in the proposed IAM structure are purely real. It is a hybrid of pseudo pilots located from the subcarriers-indices ($P = 0$ to $P = 3$) and the IAM-R scheme for the pilots located from the subcarriers-indices ($P = 4$ to $P = 7$). This scheme sets the pseudo pilots and the signs in such a way as to increase the magnitude.

The magnitude of the proposed scheme can be calculated by substituting the proposed preamble structure of Fig. 6 and the interference weights pattern (as shown in Fig. 2) in (13).

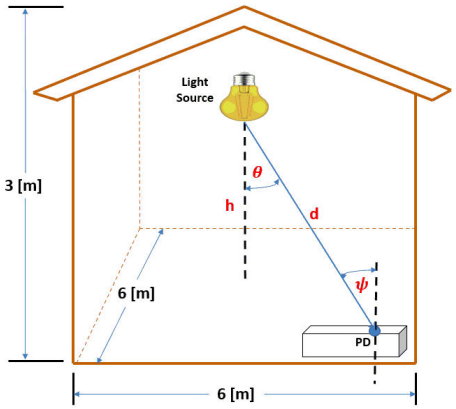

Fig. 4. Typical indoor room environment.

Table 2.
Parameters used for the VLC system.

	Parameter	Value
Source	Number of LEDs	3600 (60 × 60)
	LED transmitted power	20 mW
	Semi-angle half-power (θ)	70°
Room	Room dimensions	$6 \times 6 \times 3$ m^3
	Distance between the transmitter and the receiver plane (h)	2.25 m
Receiver	Area of the photodiode (APD)	0.001 m^2
	Field of view (FOV)	70°
	Refractive index of the lens	1.5
	Gain of the optical filter ($T_s(\psi)$)	1

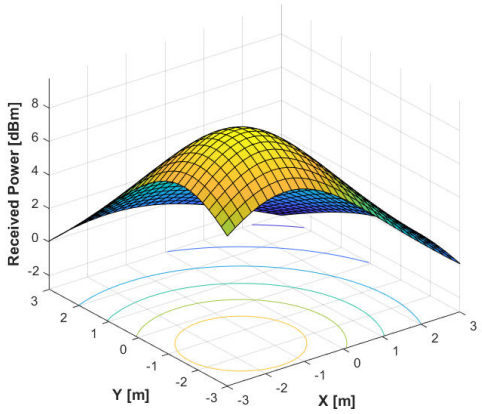

Fig. 5. Received power for the LOS path in an indoor VLC system using a single illuminating source.

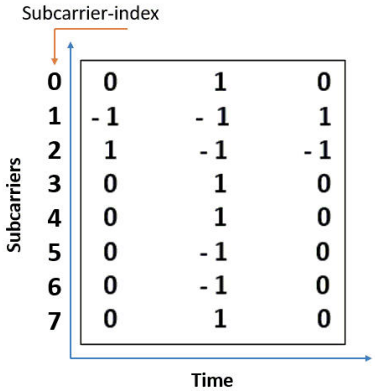

Fig. 6. Proposed IAM scheme.

The following are the calculation steps for the magnitude of the proposed IAM scheme.

The magnitude from the subcarrier-index $(P) = 0$ to 3 for the odd-indexed subcarrier is calculated by:

$$\begin{aligned}\text{Magnitude} &= \mathbb{E}\{|d \\ &\quad + j(1 * d * -\beta - 1 * d * \beta - 1 \\ &\quad * \gamma * d - 1 * \gamma * d)|^2\},\end{aligned}$$

$$\text{Magnitude} = \mathbb{E}\{|d + j(-2\beta d - 2\gamma d)|^2\},$$

$$\text{Magnitude} = \mathbb{E}\{|d - 2dj(\beta + \gamma)|^2\},$$

$$\text{Magnitude} = \sqrt{d^2 + 4d^2(\beta + \gamma)^2},$$

$$\text{Magnitude} = d\sqrt{1 + 4(\beta + \gamma)^2}. \quad (19)$$

The magnitude from the subcarrier-index $(P) = 0$ to 3 for the even-indexed subcarrier is calculated by:

$$\begin{aligned}\text{Magnitude} &= \mathbb{E}\{|d \\ &\quad + j(-1 * d * -\beta + 1 * d * \beta - 1 \\ &\quad * \gamma * d - 1 * \gamma * d)|^2\},\end{aligned}$$

$$\text{Magnitude} = \mathbb{E}\{|d + j(2\beta d - 2\gamma d)|^2\},$$

$$\text{Magnitude} = \mathbb{E}\{|d + 2dj(\beta - \gamma)|^2\},$$

$$\text{Magnitude} = \sqrt{d^2 + 4d^2(\beta - \gamma)^2},$$

$$\text{Magnitude} = d\sqrt{1 + 4(\beta - \gamma)^2}. \quad (20)$$

The magnitude from the subcarrier-index $(P) = 4$ to 7 for the odd-indexed subcarrier is calculated by:

$$\text{Magnitude} = \mathbb{E}\{|d + j(1 * d * -\beta - 1 * d * \beta)|^2\},$$

$$\text{Magnitude} = \mathbb{E}\{|d + j(-2\beta d)|^2\},$$

$$\text{Magnitude} = \sqrt{d^2 + 4d^2\beta^2},$$

$$\text{Magnitude} = d\sqrt{1 + 4\beta^2}. \quad (21)$$

The magnitude from the subcarrier-index $(P) = 4$ to 7 for the even-indexed subcarrier is calculated by:

$$\text{Magnitude} = \mathbb{E}\{|d + j(-1 * d * -\beta + 1 * d * \beta)|^2\},$$

$$\text{Magnitude} = \mathbb{E}\{|d + j(2\beta d)|^2\},$$

$$\text{Magnitude} = \sqrt{d^2 + 4d^2\beta^2},$$

$$\text{Magnitude} = d\sqrt{1 + 4\beta^2}. \quad (22)$$

As mentioned before in section 5, one of the main constraints for VLC system is that the transmitted signal must be real and positive. DC-bias optical FBMC (DCO-FBMC) can be considered the earliest variants of the optical FBMC. This technique involves applying a sufficient amount of DC bias to a bipolar signal to produce a non-negative valued signal (i.e., unipolar). DCO-FBMC is a powerful modulation technique which has suitable bandwidth efficiency but consumes a lot of power. Therefore, it was very important to develop a new approach with high spectral efficiency in addition to energy savings.

Here, as shown in Fig. 7, Flip-FBMC is introduced after converting the complex time signal (i.e., the output of SFB on the transmission side) into real and imaginary parts. The imaginary part is also converted into the real part. Finally, the two parts are consecutively merged, but it has negative values. Flip-FBMC is made by isolating the positive and negative components. Then, the negative components are flipped so that they are positive. The signal is now unipolar after merging the positive and flipping negative parts.

Then, the transmitted signal via optical channel is real and unipolar due to the optical LED. On the reception side, the optical photo detector will receive this optical signal to be converted into an electrical one and the second positive part (i.e., which is basically negative) is flipped back (i.e., negative). After this, the first part (i.e., positive sign) is merged with the flipped negative component. Thus, the bipolar signal is retrieved. Also, the same approach was used to retrieve the complex time signal (i.e., the input for AFB on the reception side). The simulation parameters of the FBMC system are shown in Table 3.

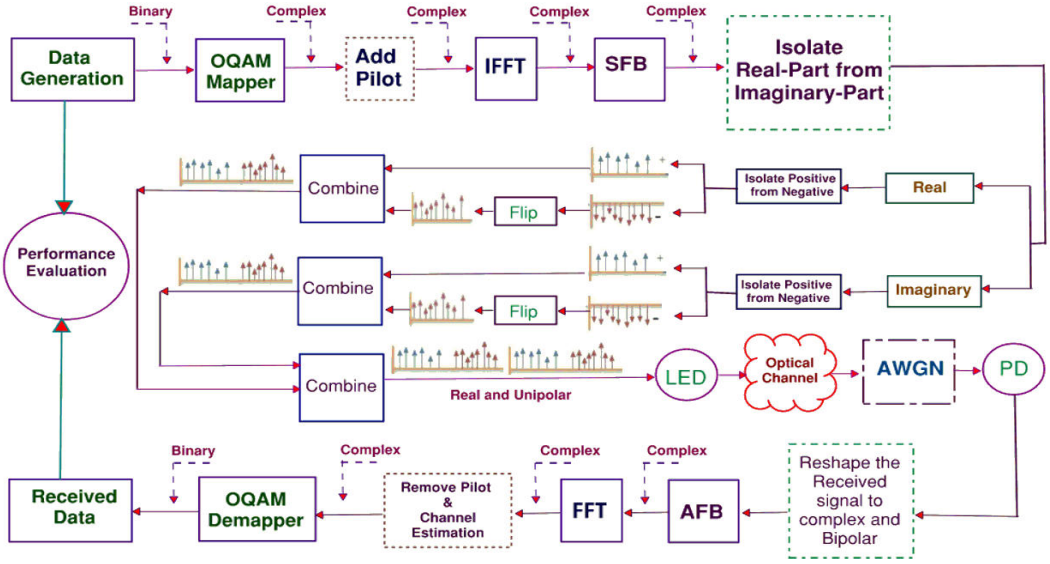

Fig. 7. Proposed F-FBMC-based VLC system with novel or conventional IAM preamble scheme.

Table 3.
FBMC system parameters.

Parameter	Value
FFT and IFFT size	512, 2048
Number of subcarriers (N)	512, 2048
Number of symbols per subcarrier (Ns)	40
Number of bits per each complex symbol	2
Prototype filter	Raised Cosine filter
Roll off factor	1
Overlapping factor (K)	4
Channel model	IEEE 802.15.7 indoor VLC standard

7. Simulation results and discussion

7.1. Power consumption

The main purpose for selecting F-FBMC is to make the transmitted signals suitable for intensity modulation / direct detection (IM/DD) and reduce the power consumption for conventional FBMC. Table 4 shows the average power consumed for each IAM-scheme (i.e., applied in both FBMC and F-FBMC). The results show that F-FBMC is more efficient than a conventional FBMC in terms of the power consumption. Also, using F-FBMC with VLC system for illumination and communication reduces the overall power consumption.

Table 4.
Power consumption for F-FBMC and FBMC.

	Proposed	IAM-R	M-IAM	NPS	E-IAM-C	IAM-C
Flip FBMC	20.77	20.66	20.77	21.06	20.77	20.53
FBMC	26.79	26.68	26.79	27.08	26.79	26.55

7.2. NMSE calculations

According to (23), the normalized mean square error (NMSE) is defined as follows:

$$\mathrm{NMSE} = \frac{1}{N}\sum_{m=0}^{N}\frac{\|H-\hat{H}\|^2}{\|H\|^2}, \tag{23}$$

where H and $\hat{H}$ are the channel and estimated channel frequency response (CFR), respectively.

Figures 8 and 9 depict the proposed IAM scheme NMSE performance in comparison to the previous preamble structures such as IAM-R, M-IAM, NPS, E-IAM-C, and IAM-C for $N = 512$ and $N = 2048$, respectively. The results show that the proposed IAM structure improves the NMSE performance effectively.

It is obvious that the proposed IAM structure has a gain of 2 dB over IAM-R and 4 dB over M-IAM (i.e., the nearest curves of other structures) at NMSE of 10^{-2} for $N = 512$. Also, it is shown that it has a gain of 2 dB over IAM-R and M-IAM at NMSE of 10^{-2} for $N = 2048$.

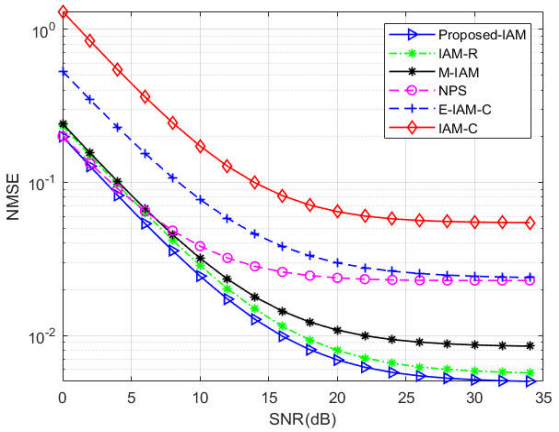

Fig. 8. NMSE of IAM structures in indoor VLC channel model for $N = 512$.

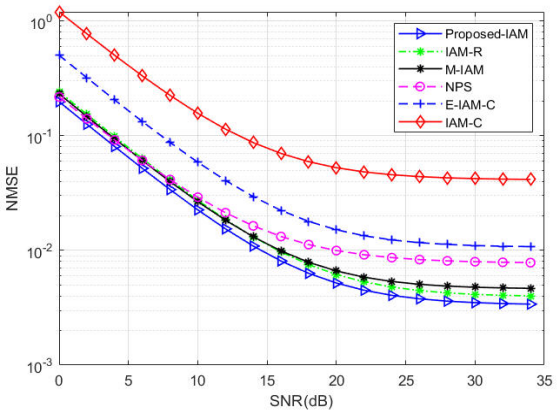

Fig. 9. NMSE of IAM structures in indoor VLC channel model for $N = 2048$.

7.3. Bit error rate (BER) performance evaluation

Also, Figures 10 and 11 show the BER performance of the proposed structure in comparison with other preamble schemes.

From Fig. 10, the BER performance of the proposed IAM structure has a gain of 0.5 dB over the M-IAM and 1 dB over IAM-R at BER of 10^{-3} for $N = 512$. Also, it has a gain of 2 dB over IAM-R and M-IAM at BER of 10^{-4} for $N = 512$.

For $N = 2048$ as shown in Fig. 11, the proposed scheme has a gain of 0.5 dB over IAM-R and 1 dB over M-IAM at BER of 10^{-3}.

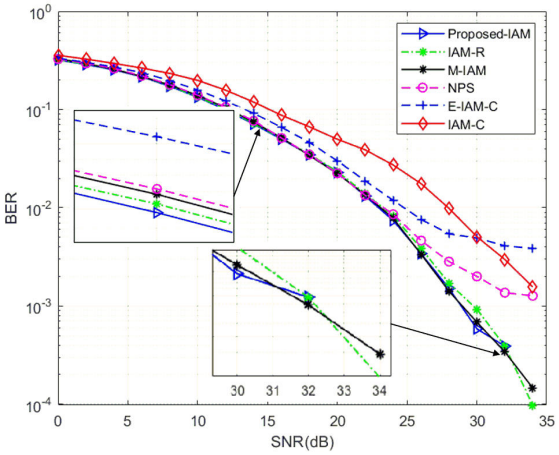

Fig. 10. BER performance of IAM preamble schemes in indoor

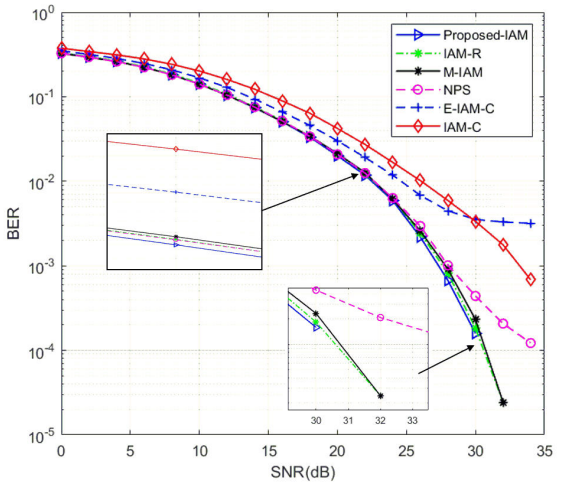

Fig. 11. BER performance of IAM preamble schemes in indoor VLC channel model for $N = 2048$.

Also, at BER of 10^{-4} compared to previous schemes, the proposed scheme can solve all errors and estimate the indoor VLC channel effectively.

7.4. Constellation diagram

The FBMC uses OQAM to modulate and demodulate the signal, and a comparison of the received signal constellation diagrams after CFR estimation using different IAM preamble schemes is shown in Figs. 12 and 13 for $N = 512$ and 2048, respectively.

Figure 12(a) presents the samples mapped on the constellation diagram at the transmitter, which are affected by the indoor VLC channel response. The four blue dots represent the ideal magnitude and phase for each of the 4 modulated symbols. On the reception side, the scatter plot does not look exactly like a signal constellation. Where the signal constellation has 4 precisely located points, the noise causes a small cluster of points to appear on the scatter plot approximately where each constellation point would be. The receiver using the preamble structures tries to estimate the CFR and eliminate the effect of that channel. Figures 12(b) to 12(g) show the scatter plots for competing IAM schemes.

It can be seen that the scatter plot of the proposed IAM structure [Fig. 12(b) for $N = 512$ and Fig. 13(a) for $N = 2048$] is more aggregated compared to other IAM schemes, allowing for a high-quality recovery of the data.

8. Conclusions

In this paper, authors have proposed and evaluated a novel IAM-preamble scheme for F-FBMC under VLC channel model. Decreasing the average transmitted power is one of the main advantages of using F-FBMC instead of the conventional FBMC (i.e., which meets the 5G requirement). Also, the illumination performance was investigated for the proposed room with LOS configuration which shows good performance across the room. The proposed structure is characterized by a pseudo pilot which has larger magnitude when compared with other schemes mentioned in the literature. The performance evaluation of the proposed IAM structure is validated through 512 and 2048 subcarriers. Compared to the conventional IAM

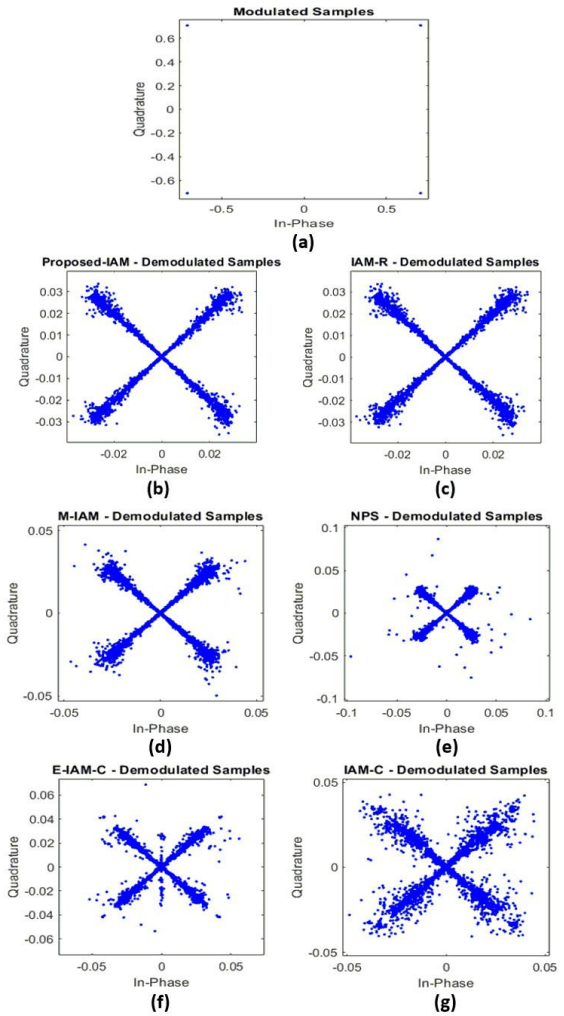

Fig. 12. Comparison of constellation diagrams for different IAM preamble schemes in indoor VLC channel model for $N = 512$.

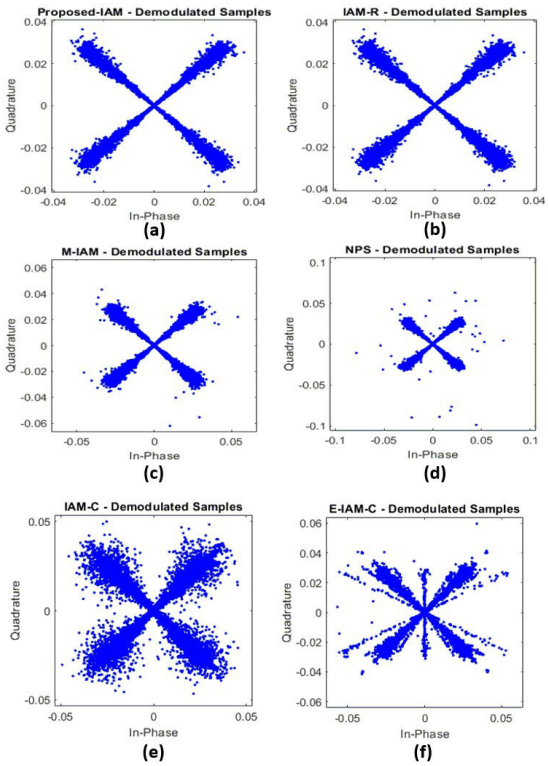

Fig. 13. Comparison of constellation diagrams for different IAM preamble schemes in indoor VLC channel model for $N = 2048$.

structures, the proposed scheme obtains a better performance in terms of NMSE and BER. Simulation results validate the improved performance via indoor VLC channel model.

References

[1] Kumar, S. & Singh, P. Filter bank multicarrier modulation schemes for visible light communication. *Wirel. Pers. Commun.* **113**, 2709–2722 (2020). https://doi.org/10.1007/s11277-020-07347-6

[2] Wang, J. Y. *et al.* Performance analysis and improvement for secure vlc with slipt and random terminals. *IEEE Access* **8**, 73645–73658 (2020). https://doi.org/10.1109/ACCESS.2020.2988470

[3] Chen, R. *et al.* Visible light communication using DC-biased optical filter bank multi-carrier modulation. in *2018 Global LIFI Congress (GLC)* 1–6 (2018). https://doi.org/10.23919/GLC.2018.8319094

[4] Al Hammadi, A., Sofotasios, P. C., Muhaidat, S., Al-Qutayri, M. & Elgala, H. Non-orthogonal multiple access for hybrid VLC-RF networks with imperfect channel state information. *IEEE Trans. Veh. Technol.* **70**, 398–411 (2021). https://doi.org/10.1109/TVT.2020.3044837

[5] Tanaka, Y., Komine, T., Haruyama, S. & Nakagawa, M. Indoor visible communication utilizing plural white LEDs as lighting. in *12th IEEE International Symposium on Personal, Indoor and Mobile Radio Communications (PIMRC)* F81–F85 (2001). https://doi.org/10.1109/PIMRC.2001.965300

[6] Mohammed, N. A., Elnabawy, M. M. & Khalaf, A. A. M. PAPR reduction using a combination between precoding andnon-linear companding techniques foraco-ofdm-based VLC systems. *Opto-Electron. Rev.* **29**, 59–70 (2021). https://doi.org/10.24425/opelre.2021.135829

[7] Qasim, A. A., Abdullah, M. F. L. & Talib, R. Adaptive DCO-FBMC in visible light communication. in *IOP Conferene: Material Science and Engineering* 812018 (2020). https://doi.org/10.1088/1757-899X/767/1/012018

[8] Kumar, S. & Singh, P. Spectral efficient asymmetrically clipped hybrid FBMC for visible light communication. *Int. J. Opt.* **2021**, (2021). https://doi.org/10.1155/2021/8897928

[9] Abouldahab, M. A., Fouad, M. M. & Roshdy, R. A. A proposed preamble based channel estimation method for FBMC in 5G wireless channels. in *35th IEEE National Radio Science Confernce (NRSC)* 140–148 (2018). https://doi.org/10.1109/NRSC.2018.8354382

[10] Roshdy, R. A., Aboul-Dahab, M. A. & Fouad, M. M. A modified interference approximation scheme for improving preamble based channel estimation performance in FBMC system. *Int. J. Comput. Networks Commun.* **12**, 19–35 (2020). https://doi.org/10.5121/ijcnc.2020.12102

[11] Sun, J. *et al.* Channel estimation approach with low pilot overhead in FBMC/OQAM Systems. *Wirel. Commun. Mob. Comput.* **2021**, 5533399 (2021). https://doi.org/10.1155/2021/5533399

[12] Liu, W., Schwarz, S., Rupp, M. & Jiang, T. Pairs of pilots design for preamble-based channel estimation in OQAM/FBMC systems. *IEEE Wirel. Commun. Lett.* **10**, 488–492 (2021). https://doi.org/10.1109/lwc.2020.3035388

[13] El-Ganiny, M. Y., Klialaf, A. A. M., Hussein, A. I. & Hamed, H. F. A. A preamble based channel estimation methods for FBMC waveform: A comparative study. *Procedia Comput. Sci.* **182**, 63–70 (2020). https://doi.org/10.1016/j.procs.2021.02.009

[14] Kong, D. *et al.* Preamble-based MMSE channel estimation with low pilot overhead in MIMO-FBMC systems. *IEEE Access* **8**, 148926–148934 (2020). https://doi.org/10.1109/ACCESS.2020.3015809

[15] Hu, S. *et al.* Training sequence design for efficient channel estimation in MIMO-FBMC systems. *IEEE Access* **5**, 4747–4758 (2017). https://doi.org/10.1109/ACCESS.2017.2688399

[16] Wang, H. Sparse channel estimation for MIMO-FBMC/OQAM wireless communications in smart city applications. *IEEE Access* **6**, 60666–60672 (2018). https://doi.org/10.1109/ACCESS.2018.2875245

[17] Lélé, C., Javaudin, J. P., Legouable, R., Skrzypczak, A. & Siohan, P. Channel estimation methods for preamble-based OFDM/OQAM modulations. *Eur. Trans. Telecommun.* **19**, 741–750 (2008). https://doi.org/10.1002/ett.1332

[18] Du, J. & Signell, S. Novel preamble-based channel estimation for OFDM / OQAM systems. in *2009 IEEE International Conference on Communications* 1–6 (2009). https://doi.org/10.1109/ICC.2009.5199226

[19] Kofidis, E. & Katselis, D. Improved interference approximation method for preamble-based channel estimation in FBMC/OQAM. in *European Signal Processing Conference* 1603–1607 (2011). https://doi.org/10.5281/zenodo.42712

[20] Wang, H., Du, W. & Xu, L. Novel preamble design for channel estimation in FBMC/OQAM systems. *KSII Trans. Internet Inf. Syst.* **10**, 3672–3688 (2016). https://doi.org/10.3837/tiis.2016.08.014

[21] Kashani, M. A. & Kavehrad, M. On the performance of single- and multi-carrie modulation schemes for indoor visible light communication systems. in *2014 IEEE Global Communications Conference (GLOBECOM)* 2084–2089 (2014). https://doi.org/10.1109/GLOCOM.2014.7037115

[22] Rehman, S. U., Ullah, S., Chong, P. H. J., Yongchareon, S. & Komosny, D. Visible light communication: A system perspective—Overview and challenges. *Sensors* **19**, 1153 (2019). https://doi.org/10.3390/s19051153

[23] Al-Ahmadi, S., Maraqa, O., Uysal, M. & Sait, S. M. Multi-user visible light communications: State-of-the-art and future directions. *IEEE Access* **6**, 70555–70571 (2018). https://doi.org/10.1109/ACCESS.2018.2879885

[24] Shalaby, E. M., Dessouky, M. & Hussin, S. Performance evaluation of UFMC-based VLC systems using a modified SLM technique. *Opto-Electron. Rev.* **29**, 85–90 (2021). https://doi.org/10.24425/opelre.2021.135832

[25] Hussin, S. & Shalaby, E. M. Performance analysis of DFT-S-OFDM waveform for Li-Fi systems. *Opto-Electron. Rev.* **29**, 167–174 (2021). https://doi.org/10.24425/opelre.2021.139753

[26] Qasim, A. A., Mohammedali, H. N., Abdullah, M. F. L., Talib, R. & Dhaam, H. Z. Enhanced Flip-FBMC visible light communication model. *Indones. J. Electr. Eng. Comput. Sci.* **23**, 1783–1793 (2021). https://doi.org/10.11591/ijeecs.v23.i3.pp1783-1793

[27] Elgala, H., Mesleh, R., Haas, H. & Pricope, B. OFDM visible light wireless communication based on white LEDs. in *IEEE Vehicular Technology Conference (VTC)* 2185–2189 (2007) https://doi.org/10.1109/VETECS.2007.451

[28] Yesilkaya, A., Karatalay, O., Ogrenci, A. S. & Panayirci, E. Channel estimation for visible light communications using neural networks. in *International Joint Conference on Neural Networks* (*IJCNN*) 320–325 (2016). https://doi.org/10.1109/IJCNN.2016.7727215